Published in final edited form as:
Adv Funct Mater. 2012 August 7; 22(15): 3170–3180. doi:10.1002/adfm.201200052.

Biomimetic Design of Protein Nanomaterials for Hydrophobic Molecular Transport

Dongmei Ren[1], **Mercè Dalmau**[1], **Arlo Randall**[2,3], **Matthew M. Shindel**[1,4], **Pierre Baldi**[2,3], and **Szu-Wen Wang**[1,*]

[1]Department of Chemical Engineering and Materials Science, University of California, 916 Engineering Tower, Irvine, CA 92697-2575

[2]School of Information and Computer Sciences, University of California, Irvine

[3]Institute for Genomics and Bioinformatics, University of California, Irvine

[4]Department of Chemical Engineering, Center for Molecular and Engineering Thermodynamics, University of Delaware, Newark, DE, 19716-3110

Abstract

Biomaterials such as self-assembling biological complexes have demonstrated a variety of applications in materials science and nanotechnology. The functionality of protein-based materials, however, is often limited by the absence or locations of specific chemical conjugation sites. In this investigation, we developed a new strategy for loading organic molecules into the hollow cavity of a protein nanoparticle that relies only on non-covalent interactions, and we demonstrated its applicability in drug delivery. Based on a biomimetic model that incorporates multiple phenylalanines to create a generalized binding site, we retained and delivered the antitumor compound doxorubicin by redesigning a caged protein scaffold. Through an iterative combination of structural modeling and protein engineering, we obtained new variants of the E2 subunit of pyruvate dehydrogenase with varying levels of drug-carrying capabilities. We found that an increasing number of introduced phenylalanines within the scaffold cavity generally resulted in greater drug loading capacities. Drug loading levels could be achieved that were greater than conventional nanoparticle delivery systems. These protein nanoparticles containing doxorubicin were taken up by breast cancer cells and induced significant cell death. Our novel approach demonstrates a universal strategy to design *de novo* hydrophobic binding domains within protein-based scaffolds for molecular encapsulation and transport, and it broadens the ability to attach guest molecules to this class of materials.

Keywords

biomimetic material; protein cage; bionanotechnology; drug delivery; hydrophobicity

[*]Corresponding author wangsw@uci.edu Phone: 949-824-2383 Fax: 949-824-2541.

Supporting Information Available: Methods and additional data for (1) structure modeling (Figure SI-1); (2) prioritizing and selecting individual sites for single variants (Table SI-1), double variants (Table SI-2), triple variants (Table SI-3), and quadruple variants (Table SI-4); and (3) protein expression (Figure SI-2); (4) protein thermostability screening (Figure SI-3); (5) protein purification (Figure SI-4); (6) particle size and TEM of DOX-4G (Figure SI-5); (7) hydrophobic surface area regions (Figure SI-6); and (8) mutagenesis protocol and oligonucleotide sequences used for mutagenesis (Table SI-5).

INTRODUCTION

Protein-based biomaterials are an important class of materials at the intersection of nanotechnology and bioengineering. Their intrinsic advantages include synthesis in natural sources, precise size and uniformity, bio-compatibility and biodegradation. The scope of these materials has been diversified by functionalizing with various metals, polymers, peptides, and protein complexes.[1] Protein materials including virus-like particles, silk proteins, synthetic peptide blocks[2, 3] and elastin-like polypeptides have been extensively utilized in applications including materials synthesis,[4, 5] cell recognition,[6] drug delivery,[7] encapsulation of guests,[8] fabrication of nanoscale arrays,[9] and tissue engineering. Protein engineering and chemical synthesis provides these biomaterials with powerful tools to control molecular structures, multiple functionalities, and biological features.[10] To enable transport of small organic molecules by protein systems, the molecules are frequently covalently conjugated to their protein carriers.[7, 11–13] This has been a useful strategy; however, it can limit broader applicability if the molecule does not have functional groups available for conjugation or if the protein scaffold has limited or no unique attachment sites.

In this investigation, we demonstrate the feasibility of a new strategy to encapsulate guest molecules in a protein-based material by designing hydrophobic interactions, thereby circumventing the limitations of conventional chemical conjugation. Because hydrophobic molecules are the primary constituents of small molecule drugs that have emerged from high-throughput screening,[14, 15] such an approach would be relevant for a broad class of organic molecules. Inspired by multi-drug efflux transporters, we implemented a biomimetic approach to enhance hydrophobic drug-protein interactions. Multi-drug efflux transporters (e.g., P-glycoprotein) are usually protein complexes that transport a broad range of structurally divergent organic molecules out of cells,[16] and they can contribute to multi-drug resistance in cancer treatment.[17] More than 100 pharmaceutically-active molecules have been identified that can bind to P-glycoprotein.[16, 18, 19] Most of these substrates are either amphiphilic or have a significant amount of accessible hydrophobic surface area, suggesting that hydrophobic interactions play an important role in binding. In fact, the crystallographic structure of AcrB, a multi-drug efflux pump in *E. coli*, shows that the determinant of the protein's broad specificity is a binding site that involves primarily non-specific hydrophobic and aromatic **π-π** interactions from 12 conserved phenylalanines (Phe)[20] (one of the most hydrophobic amino acids). The critical role of Phe residues residing in a large binding site is also supported by mutagenesis studies and a low-resolution structure of P-glycoprotein.[21, 22] We therefore speculated that a protein nanoassembly could be designed to encapsulate and transport molecules by introducing Phe to increase the accessible hydrophobic surface area of the protein nanoparticle.

To test our hypothesis, we redesigned a model protein scaffold, the E2 component of the pyruvate dehydrogenase multienzyme complex. The structural core of E2 is a self-assembling, 25-nm hollow nanoparticle with an architecture resembling virus-like particles.[23, 24] This scaffold can be re-engineered at different interfaces to couple drug molecules,[11] modify assembly behavior,[25, 26] and modulate immunological responses.[27] Other caged protein assembly systems have been widely investigated as nanoparticulate carriers for the delivery of molecular therapeutics and as constrained containers for materials applications.[28–30] The potential of protein complexes as molecular carriers stems from their nanoscale size range, precise molecular tunability through recombinant technology and chemical synthesis, and self-assembly behavior.

In this study, we increased the hydrophobicity of E2's hollow cavity surface by systematically introducing Phe mutations. This approach has the potential to significantly

increase the drug loading capacity beyond levels achieved by conventional covalent attachment to the cavity surface or encapsulation in a polymeric matrix of comparable size; the hydrophobic regions within the cavity can potentially serve as binding and nucleation sites for solid-state crystallization of the organic guest molecules, and the empty interior space would be fully available to accommodate these molecules. For our target guest molecule, we chose doxorubicin (DOX), an anti-tumor chemotherapeutic commonly used as a model compound in drug delivery and formulation investigations.[12, 31–33] While DOX has both hydrophilic and hydrophobic molecular components, it is conventionally considered hydrophobic, with a log P value of 0.71 at pH 7.2.[34] Furthermore, DOX is a P-gp substrate,[35] which is relevant given that multi-drug efflux transporters are our biomimetic model for drug-protein interactions.

Our study is the first to create non-native, hydrophobic solvent-exposed surfaces into a protein-based material for general molecular encapsulation. We quantify the extent to which DOX is loaded within our engineered protein cavity and demonstrate the potential therapeutic applicability of the resulting drug-protein complex by examining delivery and cytotoxicity to breast cancer cells. Although we have re-engineered a specific model protein, our strategy can be generally applied to other protein systems to introduce *de novo* hydrophobic binding domains for guest molecule attachment.

RESULTS AND DISCUSSION

Selection and screening of protein nanoparticles with multiple phenylalanines

The E2 protein nanoparticles are recombinant biomaterials synthesized in *E. coli*, as described in the Experimental Section. An iterative approach was used to select and create variants (i.e., mutants) of the E2 nanoparticle with one to four Phe introduced per subunit for increasing accessible hydrophobic surface area. Because the E2 protein nanoparticle consists of 60 identical subunits, single-, double-, triple-, and quadruple-Phe mutations generate 60, 120, 180, and 240 mutations per E2 scaffold, respectively. Figure 1 depicts one representative variant of a quadruple-Phe nanoparticle (designated as 4-G) and shows that changes in hydrophobicity are designed into the internal hollow cavity.

The final list of 37 variants that was experimentally synthesized, cloned, and screened for expression and thermostability is given in Table 1. Priority scores from molecular calculations and representative expression and thermostability screening results for variants are presented in Supporting Information (Priority ranking results, Tables SI-1 to SI-4, and Figures SI-2, SI-3). Results of these nanoparticle variants were compared to nanoparticles with native, wild-type E2 sequence (E2-WT, control). The E2-WT nanoparticle contains six native Phe per subunit, but these are generally dispersed, buried in the complex, and not surface-accessible.

Our cell lysate screens showed that the introduction of more mutations generally correlated with decreased protein expression (in *E. coli*) and decreased stability (Supporting Information). Protein particles with one and two Phe mutations per subunit (60 and 120 mutations per scaffold) yielded both expression and thermostability levels close to those for the E2-WT scaffold. Modest decreases in expression and thermostability were observed as the number of Phe mutations increased to three (180 Phe per scaffold), and these decreases were even more significant for quadruple variants (240 Phe within the cavity).

Structure and thermostability of purified protein nanoparticles with multiple phenylalanines

Based on expression levels, thermostability, and structural variability, we chose two single (1-C and 1-F), one double (2-I), four triple (3-E, 3-G, 3-H, and 3-J), and four quadruple (4-

A, 4-C, 4-D, and 4-G) variants for further purification and characterization. Scale-ups of 4-A and 4-C yielded inadequate protein expression for further processing, but the remaining variants were purified. Purification results from one representative nanoparticle variant, 4-G, are presented in Figure SI-4. Drug encapsulation within the hollow cavity requires intact and stable dodecahedral protein assemblies, and we confirmed these properties for the purified Phe variants. Figure 2 shows hydrodynamic diameter, thermostability analysis, and structural confirmation for the representative variant 4-G (K239F-E375F-R380F-D381F). A summary of the size and stability characterization for all the purified Phe variants and the E2-WT control (no mutations) is given in Table 2.

Our data show the correct 60-mer assembly of each different variant and their high thermostability. Average hydrodynamic diameters ranged between 25.9 ± 1.0 nm and 32.7 ± 1.1 nm, close to that of E2-WT (26.9 ± 0.7 nm). The structures of individual nanoparticles were observed by TEM (Figure 1C). Average midpoint temperatures of unfolding (T_m) ranged from 83.3 °C to 90.6 °C, and the average onset temperature of unfolding (T_o) was from 66.7 °C to 79.8 °C. In comparison, the E2-WT control averaged T_m = 90.1 °C and T_o = 79.2 °C. Although the quadruple Phe variants yielded T_o values noticeably lower than the others, these unfolding temperatures are still much higher than typical proteins. Reduced stability as the number of Phe on solvent-accessible surfaces increased (e.g., the hollow cavity of the E2 dodecahedron) is not unexpected, as hydrophobic residues are typically buried within the folded protein to contribute to the protein stability.[37]

Drug encapsulation in purified variant nanoparticles

To investigate the effect of increasing hydrophobicity on drug encapsulation, DOX was incubated with the protein nanoparticle variants. Figure 3 presents the number of DOX molecules encapsulated per protein subunit after incubating at a 3:1 DOX:subunit incubation ratio (equivalent to 180 DOX per nanoparticle). We observed a low degree of DOX loaded into the E2-WT protein scaffold, equivalent to 0.4 ± 0.2 molecules DOX per subunit (~24 DOX molecules per nanoparticle). This result was not surprising because DOX has been reported to exhibit a small degree of background binding to serum proteins.[38, 39]

In general, the increase in drug encapsulation correlates with a larger hydrophobic surface area. The single-Phe (1-C) and double-Phe (2-I) nanoparticles exhibited DOX binding similar to the E2-WT control, with average encapsulation ratios of 0.3 ± 0.2 and 0.4 ± 0.01 DOX encapsulated per subunit, respectively (Figure 3). The single-Phe (1-F) and triple-Phe variants (3-E, 3-G, 3-H, and 3-J), encapsulated 1.5 to 2.3 times more DOX molecules than E2-WT, ranging between 0.6 to 0.9 DOX per subunit. For these triple-Phe variants, we estimated a 59–81% increase in the hydrophobic surface area within the hollow cavity relative to E2-WT (Figure 4). The results of the quadruple-Phe variants (4-D, 4-G) are particularly interesting, as they exhibited a substantial increase in the degree of drug complexation over the triple-Phe variants. Nanoparticles 4-D and 4-G loaded 1.8 ± 0.3 and 2.0 ± 0.4 DOX molecules per protein subunit, respectively, which are approximately five times more than the amount of drug relative to the E2-WT. The estimated increases in hydrophobic surface area within the cavity relative to E2-WT are 83% and 118% for 4-D and 4-G, respectively.

Given the geometry of the scaffold and the relatively long-range nature of the hydrophobic interaction, it is likely that DOX molecules which diffuse into the cavity of the hydrophobic variants will be attracted to the cavity's surface. Because the introduction of Phe occur in the hollow cavity of the scaffold, and the dodecahedral structures have been confirmed intact, the measured increases in drug-protein complexation relative to E2-WT can be attributed to the Phe differences within the hollow cavity of the scaffold. Further evidence of DOX encapsulated inside the hollow cavity is shown in Figure SI-5 (Supporting Information),

which demonstrates that the hydrodynamic diameters of the protein assemblies remain the same after drug complexation at different incubation ratios. Transmission electron microscopy supports the DLS data, confirming the intact structure and size of the drug-loaded protein particles (Figure SI-5, panel D).

The sharp increase in the amount of DOX encapsulated between the triple and quadruple variants suggests that a critical hydrophobic surface area is needed. However, we note that the differences in hydrophobic surface area between 3-H and 3-G compared to 4-D are not significant (Figure 4). Therefore, our data indicates that in addition to a *minimum* amount of total hydrophobic surface area, the specific locations of Phe mutations and the formation of larger contiguous hydrophobic surface areas in multi-site mutations are also important. In fact, variant 4-D contains a large contiguous hydrophobic surface area of 1635 $Å^2$, which is clearly identifiable upon visual inspection (Figure SI-6, Supporting Information). This region spans three subunits at the three-fold axis of symmetry, and thus contains 12 Phe mutations. The hydrophobic surface area (which is non-contiguous) formed by the corresponding residues in the E2-WT is only 343 $Å^2$. In variant 4-G, the boundaries of the largest contiguous area are not easily defined; however, it is clear that Phe mutations from subunits which share an interface at the three-fold axis of symmetry can be part of the same contiguous hydrophobic surface area (e.g. positions 239 and 375 of one subunit with positions 380 and 381 of another subunit) (Figure SI-6, Supporting Information).

To examine our hypothesis that hydrophobic interactions play an important role in DOX loading, we incubated other hydrophobic molecules (Nile red and rhodamine B base) with the 4-G variant and E2-WT. Nile red is very hydrophobic (<1 μg/mL solubility in water[40]) and rhodamine B is a P-glycoprotein inhibitor,[41] which is relevant since multi-drug efflux transporters are our biomimetic model for drug-protein interactions. For Nile red, the fluorescence intensity of 4-G was 3.8 times higher than for E2-WT. Furthermore, the fluorescence intensity of rhodamine B in 4-G averaged 56 times more than that of E2-WT. Therefore, both dyes showed preferential complexation with the 4-G mutant relative to the E2-WT scaffold. These results support the mechanism of hydrophobic interactions to encapsulate guest molecules into our multiple-Phe protein scaffolds and the potential applicability toward other hydrophobic drug molecules.

Hydrophobic drug loading in quadruple-phenylalanine nanoparticle

Based on the drug loading results in the multiple-Phe nanoparticles, further investigations of protein-drug complexation focused on the quadruple variants. Both 4-D and 4-G yielded intact, stable nanoparticles (Table 2, Figure 1) and loaded DOX at comparable levels (Figure 3). However, while we could obtain 4-G to >95% purity (Figure SI-4), the purity of 4-D ranged between ~60–80% over several batches due to the lower protein expression levels upon scale-up. For this reason, we present further drug loading data for the 4-G variant (K239F-E375F-R380F-D381F), which contains the 240 Phe mutations within the internal cavity highlighted in Figure 1.

Enhancement of drug loading level—Our drug loading investigations to identify high-loading protein nanoparticles were performed at a DOX:subunit incubation ratio of 3:1 (Figure 3). To determine whether the loading level could be increased, we incubated 4-G and the E2-WT control at DOX:subunit incubation ratios of 3:1, 10:1, and 20:1. DOX has a relatively low aqueous solubility,[42] and consistent with this, we observed that DOX precipitated upon increasing the ratio beyond 20:1. Figure 5 shows the resulting drug loading amounts after free, unbound DOX molecules were removed. The hydrophobic cavity of the 4-G variant encapsulated significantly more DOX molecules relative to E2-WT as incubation ratio is increased. Incubation ratios of 3:1, 10:1, and 20:1 produced drug

encapsulation ratios of 2.0 ± 0.4, 5.5 ± 0.3, and 6.5 ± 0.2 DOX per subunit (corresponding to 129, 330, and 390 DOX molecules per nanoparticle), respectively, for variant 4-G. In contrast, the amount of DOX per subunit for E2-WT was 0.3 ± 0.2, 0.2 ± 0.3, and 0.8 ± 0.01, for the respective 3:1, 10:1, and 20:1 incubation ratios. Therefore, 4-G exhibited up to an approximate 30-fold increase in drug encapsulation relative to native E2. The average particle size of the nanoparticle after drug encapsulation remained the same regardless of incubation ratio (Figure SI-5), demonstrating that the structure of protein scaffold remained intact and drug loading occurs inside the cavity.

Doxorubicin has both hydrophobic and hydrophilic components, but is typically considered to be a model hydrophobic molecule in therapeutic delivery[43, 44] with a less-than-ideal solubility for drug formulations (0.1 mg/ml in phosphate buffer).[42] Using our intermediate encapsulation amount of 5.5 DOX per subunit (for the 10:1 molar incubation ratio) and the calculated volume of the hollow nanoparticle cavity,[23] the introduction of hydrophobic sites in the 4-G variant gives a local DOX concentration of ~370 mg/ml inside the cavity, which is several orders of magnitude above its free solubility in aqueous solution, suggesting nucleation of solid-state DOX in the cavity. Furthermore, 4-G also demonstrates at least a six-fold higher amount of DOX encapsulation over the conventional strategy of attachment using chemical conjugation.[7, 11]

We calculate that the DOX amount loaded in this investigation reached up to 390 DOX molecules per nanoparticle or ~13.4 wt%. This is generally higher than loading levels of other polymeric nanoparticles in drug delivery, which typically range from 2% to 12%.[45–48] The theoretical maximum encapsulation ability of the E2 cavity is approximately 1300 DOX molecules (44.9 wt%), based on crystallographic data of the drug[49] and the E2 protein complex,[50] suggesting that additional loading enhancement can potentially be achieved. Our work here is a significant first step in showing that the general strategy of engineering hydrophobicity can be used to nucleate and hold organic molecules.

Retention of drug in protein nanoparticle—We investigated the retention of DOX within the nanocapsule in a DOX-depleted solution. We expected that if the protein-drug complex is bound by weak non-specific interactions, then DOX within the cavity should become soluble in an unsaturated solution and diffuse out of the cavity, thereby decreasing the amount of DOX within the cavity. As described in the Experimental section, we performed multiple iterations of free-drug removal and 24-hr incubation in a DOX-depleted solution with drug-loaded 4-G and E2-WT.

For E2-WT, nearly all DOX bound to the protein was removed after the second round (at 48 hrs) (Figure 6). This suggests that DOX is non-specifically and weakly bound to the E2-WT protein and that removal of initial free DOX will drive the remaining DOX into solution. In contrast, for the 4-G variant, DOX is retained at 5.5 ± 0.3, 8.6 ± 0.1, and 10.1 ± 0.2 DOX molecules per subunit after the first, second, and third 24-hr iterations, respectively.

We note that the drug loading ratios appear to increase after each iteration for 4-G (Figure 6). One possible explanation may be difference in surface protein adsorption to polystyrene surfaces between drug-loaded and unloaded proteins.[51] Examination of the data reveals that protein concentrations decrease after each 24-hr iteration. Calculations of DOX binding ratios assume that protein loss during the experimental procedures is identical for loaded and unloaded proteins. However, if the unloaded protein controls (used to determine the protein concentrations) adsorb more on polystyrene surfaces than the DOX-loaded samples, calculated loading ratios will be artificially high. An alternative explanation may be aggregation or Ostwald ripening of DOX nanoparticles within the protein cavities, which may also give rise to the anomalous increases in DOX:protein ratio. This growth in drug

nanoparticles (at the expense of smaller particles) is a common observation in drug nanosuspensions when surfactants are absent in the formulation,[52, 53] and long-term incubation of DOX with 4-G could be yielding a population of drug-protein complexes with increasingly larger DOX aggregates within the core. Others have noted that the formation of chromophore aggregates will produce a significant increase in intensity of scattered light within the range of optical wavelengths over which the molecular species absorbs.[54] Since solid DOX nanoparticles have a high refractive index estimated to be 1.71 (http://www.chemspider.com/Chemical-Structure.29400.html), their nucleation and growth over time could increase light scattering within the sample, resulting in an increase in overall optical extinction and consequently skewing the DOX:protein ratios towards higher values. Since the hydrodynamic diameter of the DOX-protein complexes does not change after the three-day incubation, any DOX nanoparticle growth due to Ostwald ripening remains inside the E2 cavity.

Regardless of the exact mechanism for the observed increase in loading, the conclusion that DOX remains complexed to the E2 cavity of the 4-G variant is supported by our data. The drug-protein interaction between 4-G and DOX is significantly more stable than E2-WT and DOX, due to the additional engineered hydrophobic interactions. DOX has previously been reported to be retained in a virus capsid, attributed to the interaction between DOX and the viral genome.[55] In contrast, our system only utilized engineered hydrophobic interactions to retain DOX in the protein nanoparticle.

Doxorubicin release in breast cancer cells

Confocal microscopy of drug-protein nanoparticle uptake—We examined the potential applicability of the drug-encapsulating protein nanoparticles. Confocal microscopy of DOX-loaded 4-G (DOX-4G) incubated with MDA-MB-231 breast cancer cells showed that the cell uptake mechanism for these particles is different than for free unconjugated DOX (Figure 7). DOX-4G were primarily localized in intracellular vesicles or organelles, and images were consistent with endosomal/lysosomal accumulation. In contrast, free DOX accumulated in both the nucleus and non-nuclear organelles of the cells. These results are consistent with prior investigations in which DOX was covalently attached to the hollow cavity of the E2 nanocapsule but released after cellular uptake,[11] and with studies using DOX-loaded polymeric nanoparticles.[46, 56, 57] From these differences between DOX-4G and free DOX, we infer that DOX is attached to the nanoparticle when it is internalized by the cell.

Dose-response results—Dose-response curves of DOX-4G showed cytotoxicity with an IC_{50} value of 0.33 ± 0.12 μM (Figure 8), revealing that DOX is released from 4-G. This toxicity value is within the range of previously-reported drug-nanoparticle studies.[57–59] In comparison, IC_{50} values of the free DOX control yielded 0.93 ± 0.30 μM, also consistent with prior reports.[11, 60, 61] These results indicate that the DOX-4G protein cages are slightly more cytotoxic than free DOX. Dose-response data for 4-G protein cages alone (no DOX) revealed no toxicity within the protein concentration range used.

The confocal images and dose response data together strongly suggest that DOX-4G is taken up as a drug-nanoparticle complex by the cells and that drug release is intracellular. According to previous investigations relating cell uptake to nanoparticle diameters, particulates at the size of our protein scaffolds are likely to be internalized by cells through receptor-mediated endocytosis.[62–64] Serum proteins in the media may also play an important role in this process by adsorbing to the DOX-4G nanoparticle surface and facilitating cellular uptake[65, 66]. The endocytic pathway undergoes a pH change as nanoparticles are delivered from typical physiological pH (pH 7.4) to the acidic environment

of the late endosome and lysosome (pH 5).[67] Therefore, since DOX is known to exhibit significantly higher solubility in acidic environments,[42, 68] one possible explanation for DOX release may be related to the pH change in the endocytic environment.

Indeed, when we incubated drug-loaded DOX-4G for 48 h at pH 5.0, we observed that ~75% of DOX was released from the nanoparticles relative to DOX-4G incubated at pH 7.4. This degree of drug release is consistent with DOX release from carbon nanotube-DOX complexes which were loaded at high pH and released at acidic pH.[69] Similar to that reported study, which utilized pH-dependent π–π interactions between carbon nanotubes and DOX to bind the drug, our DOX-protein binding is also likely promoted by π–π interactions between the Phe and DOX, enhancing hydrophobic interactions. Our biomimetic model, P-glycoprotein, in fact, is proposed to act upon structurally divergent substrates using such interactions. At acidic pH, DOX can be protonated, resulting in increased hydrophilicity, increased solubility, and reduced hydrophobic interactions with Phe, thereby being released into aqueous solution. Overall, our results show that drug-protein complexes engineered through hydrophobic interactions can be manipulated to induce significant biological effects.

CONCLUSIONS

Our study investigated the feasibility of engineering hydrophobic interactions into a general protein-based scaffold to obtain small guest molecule retention. We demonstrated that the biomimetic approach of incorporating targeted phenylalanine mutations into a protein cavity can yield stable storage of an organic molecule, and the encapsulation capacity can be several times more than the conventional strategy of chemical conjugation. These drug-loaded protein nanoparticles can be taken up by breast cancer cells, with subsequent intracellular drug release to induce cell death. This strategy of engineering non-native hydrophobicity is a novel approach that could be broadly utilized for attaching guest molecules to other protein-based materials for molecular transport and applicability in bionanotechnology.

EXPERIMENTAL SECTION

Materials

Sodium phosphate dibasic, sodium phosphate monobasic, sodium chloride (NaCl), 1 N hydrochloric acid (HCl), sodium dodecyl sulfate (SDS), *N,N*-dimethylformamide (DMF), and magnesium chloride ($MgCl_2$) were supplied by EMD. Isopropyl β-D-thiogalactopyranoside (IPTG), acetic acid, acetonitrile, formic acid, potassium phosphate monobasic, and potassium phosphate dibasic were purchased from Fisher Scientific. Dimethyl sulfoxide (DMSO) was obtained from Thermal Scientific. Restriction enzymes (NdeI, DpnI, and BamHI), T4 DNA ligase, DNase, RNase, and calf intestinal alkaline phosphatase were purchased from New England Biolabs. PfuUltra High-Fidelity DNA polymerase was from Stratagene. Dulbecco's phosphate-buffered saline (PBS), 3-(4, 5-dimethylthiazol-2-yl)-2,5-diphenyltetrazolium bromide (MTT), and Hoechst 33342, trihydrochloride trihydrate were purchased from Invitrogen. The protein molecular weight standard (Perfect Protein Marker, 10–225 kDa) was obtained from Novagen. Phenylmethylsulfonyl fluoride (PMSF) was from Pierce and sodium azide was from Merck KGaA. MDA-MB-231 breast cancer cells were purchased from ATCC. Dulbecco's Modified Eagle's Medium (DMEM) and rhodamine B base were purchased from Sigma. Fetal bovine serum (FBS) and L-glutamine were obtained from Mediatech. Nile red was from Acros Organics. Doxorubicin hydrochloride was obtained from Yic-Vic (Hong Kong) and was generously given to us by Dr. Felix Kratz. Water was purified by a Milli-Q system (Millipore) to a final resistivity of at least 18.2 MΩ-cm.

Modeling and calculation methods for selection of mutagenesis sites

Protein structure modeling—Our strategy to increase general hydrophobicity into the internal hollow cavity of the E2 protein assembly was to introduce phenylalanines (Phe). The sites for Phe mutations were selected using an iterative approach which included both structural modeling analysis and experimental data, and all the variants (i.e., mutants) experimentally constructed are summarized in Table 1. We utilized the all-atom models to calculate three structural features which contributed to the selection of variants: (1) solvent accessibility information, as calculated by the DSSP program[70] on subunit, (2) the minimum distances between pairs of residue side-chains, and (3) potential steric hindrance in variants. Details of this model are found in Supporting Information.

Ranking of single, double, triple and quadruple variants—We first developed computational metrics to prioritize individual sites and then extended these metrics for multi-site variants. A summary of the methods is given here, and additional details are given in Supporting Information. To increase the hydrophobic surface area within the hollow internal cavity, we targeted sites which: (1) are within the internal cavity, (2) are surface exposed in the complex, and (3) have hydrophilic or small side-chains to maximize hydrophobicity increases. Other criteria for elimination included residues with side-chains more than 70% buried in the complex (based on all-atom model) and sites with native hydrophobicity. Furthermore, we developed priority score equations designated as $E_{ind}(a)$, $E_{paired}(a,b)$, $E_{triplet}(a,b,c)$, and $E_{quadruplet}(a,b,c,d)$ for single, double, triple and quadruple muatants, where a, b, c, d are individual sites. These calculations considered the distance from the core, the exposure value in the complex, the charge of the residue, expression and thermostability of the variants, and diversity of the sets. All the Phe variants were constructed, expressed, and tested. A summary of all nanoparticle variants experimentally created and tested is presented in Table 1.

Experimental methods for selection of mutagenesis sites

Design and construction of phenylalanine variants—Experimental and modeling results for one set of variants (e.g., double-Phe) were used to generate the subsequent set of variants (e.g., triple-Phe). Because the E2 protein nanoparticle consists of 60 identical subunits, single-, double-, triple-, and quadruple-Phe mutations generate 60, 120, 180, and 240 mutations per E2 scaffold, respectively. Genes with Phe mutations were made as previously described using site-directed mutagenesis of the E2 gene in a pGEM-3Z vector,[24] and the protein nanoparticles were expressed using pET-11a vector in *E. coli* BL21(DE3). A more detailed DNA mutagenesis protocol is given in Supporting Information.

Protein expression and thermostability screen of all phenylalanine variants—Protein expression and thermostability were screened as described in Dalmau et al.[24] Cells with plasmids containing the E2 genes were induced with IPTG at 30 °C and 37 °C, and soluble and insoluble fractions were run on a Tris-HCl SDS-PAGE gel. Expression levels were quantified by the Analyze function in Image J using the 50 kDa band in the protein marker as a reference standard and the 28 kDa protein band from pET-11a in BL21(DE3) as background. To investigate thermostability, the soluble fractions of each variant were heated up to 40, 50, 60, 75 and 95 °C for 20 min. The denatured and aggregated proteins were removed by centrifugation, and the remaining soluble fraction was loaded on a Tris-HCl SDS-PAGE gel.

Protein nanoparticles purification

Based on the results from protein expression, stability screens and molecular modeling, a subset of nine proteins ranging in different amounts of Phe in the cavity was selected for scale-up, purification, and further characterization. Experimental protocols were based on Dalmau et al.[24] In brief, *E. coli* BL21(DE3) containing mutated E2 genes in the pET vector were grown in 1 L LB media with ampicillin at 22, 30, or 37°C, depending on maximum expression in the soluble fraction. Protein expression was induced, cells were lysed, and the E2 proteins in the soluble fractions were purified on a Q Sepharose column followed by a Superose 6 PG column. Proteins were concentrated and stored in 50 mM potassium phosphate (pH 7.4), 100 mM NaCl, 0.02% sodium azide, and 5 mM EDTA. The incorporation of the expected Phe mutations was confirmed by DNA sequencing and molecular weight (electrospray mass spectrometry). The purity of each variant was evaluated by SDS-PAGE and mass spectrometry.

Characterization of protein nanoparticles

We confirmed the molecular weight, correct protein assembly, and thermostability as previously described[11, 24] and these methods are only briefly summarized here. Hydrodynamic particle size measurements were performed by dynamic light scattering (DLS) with a Zetasizer Nano ZS (Malvern Instruments). Full complex assembly and intact structure was confirmed by a Philips CM-20 TEM using protein samples stained with 2% uranyl acetate. To confirm expression of the full-length protein and the incorporation of Phe mutations, the molecular weights of the variant proteins were evaluated by a Micromass LCT Premier Mass Spectrometer (Waters). Purity of the final purified proteins was estimated by SDS-PAGE and mass spectrometry.

Far-UV CD was used to evaluate the folding, secondary structure, and thermostability of the protein scaffolds. The midpoint of unfolding temperature (T_m) of each variant E2 complex was extracted from ellipticity (at 222 nm) vs. temperature profiles. We fit the data to a thermodynamic model developed by Greenfield[71] via a multi-parameter, non-linear regression performed using the Levenberg-Marquardt algorithm. Additionally, we computed an onset of unfolding temperature (T_o), defined as the value at which 5% of the protein molecules have unfolded. Data processing for thermostability parameters was performed in MATLAB.

Doxorubicin encapsulation screen

To screen the binding of typical hydrophobic drugs to the internal cavity of the nine purified variants, we used the anti-tumor drug doxorubicin (DOX) as the model hydrophobic drug molecule. We incubated 0.2 – 0.4 mg/mL of the purified protein variants with DOX at DOX:protein subunit incubation ratio of 3:1 at room temperature for at least 2 hrs. Incubation times beyond 2 hours did not alter final protein-drug binding ratios. After incubation, unbound DOX was removed by a desalting column (Zeba, 40 kDa MWCO, Pierce) following the vendor protocol using phosphate buffer (50 mM potassium phosphate, 100 mM NaCl, pH 7.4) as the exchange solution. We quantified the number of DOX encapsulated per protein subunit. The protein concentration was determined by a Micro BCA Protein Assay Kit (Pierce), and DOX concentration was determined by absorbance at 495 nm (SpectraMax M2, Molecular Devices) and calibrated to standard curves. The wild-type E2 protein (E2-WT) was used as the control.

Doxorubicin encapsulation by quadruple-phenylalanine variants

Based on the results from the DOX encapsulation screen, we selected the two variants with the highest encapsulation capacity for further studies, quadruple Phe variants, 4-D (D381F-

G382F-E383F-A386F) and 4-G (K239F-E375F-R380F-D381). We incubated 4-D, 4-G, and E2-WT (control) with DOX at DOX:protein subunit ratios of 3:1, 10:1, and 20:1 at room temperature for 2 hours. Excess unbound DOX was removed, and concentrations of remaining DOX and protein were determined as described above. To ensure that DOX bound to the protein did not interfere with the micro-BCA analysis, in parallel, we quantified the empty E2 variants without DOX (but processed in parallel using the identical methods) for protein concentration. Replicates of n = 3–5 were performed for each condition.

Because DOX can potentially diffuse out of the protein cavity through its 5-nm openings, we investigated the retention of drug in 4-G protein scaffold over time. We incubated 4-G with DOX at 10:1 DOX:subunit incubation ratio for 2 hrs at room temperature, stored samples at 4 °C overnight, and removed unbound DOX at 24 hr with desalting columns. Protein and DOX concentrations were measured as described above. With free DOX removed, we expected that if the DOX-protein complex is not stable, DOX will diffuse out of the protein until the DOX in solution reaches its solubility limit (~0.1 mg/ml in phosphate buffer[42]). Therefore, samples depleted of free-DOX were incubated in phosphate buffer again for another 24 hours, desalted, and quantified. This process was repeated for three rounds to yield one, two, and three iterations of free-DOX removal, corresponding to total incubation times of 24, 48 and 72 hrs, respectively. After each incubation, protein and DOX concentrations were measured.

To compare the release of DOX from 4G-DOX at different pH, we incubated 4G-DOX in potassium phosphate buffer at pH 5.0 and 7.4 for 48 hrs. The released free DOX was removed by desalting columns. The DOX concentration remained in 4G-DOX at pH 5.0 was compared to that at pH 7.4.

Imaging uptake into human breast cancer cells

To investigate the intracellular distribution of DOX conjugated to the 4-G variant (DOX-4G), we used confocal laser scanning microscopy.[11] DOX-4G was prepared at a 20:1 DOX:subunit incubation ratio, with free DOX subsequently removed. Human breast cancer cells MDA-MB-231 (10^4 per well) in growth medium (DMEM supplemented with 10% fetal bovine serum and 1% L-glutamine) were seeded in a Lab-Tek chambered coverglass (Thermo Scientific Nunc) and incubated at 37°C in 5% CO_2 for 16–20 hrs. The medium was replaced with fresh medium containing free DOX (3 μM) or DOX-4G (at final concentration of 0.012 mg/mL protein and 3 μM equivalent DOX), and cells were incubated for 56 hr. After incubation the medium containing DOX or DOX-4G was removed and cell nuclei were stained with media containing 0.5 μg/mL Hoechst 33342 for 30–60 min, and washed and covered with PBS. CLSM images were obtained using an Olympus Fluoview FV1000, at excitation/emission filter wavelengths of 635 nm/655–755 nm for DOX and 405 nm /430–470 nm for Hoechst 33342.

Cytotoxicity to human breast cancer cells

To evaluate cytotoxicity of DOX-4G, we used an MTT assay to determine the dose response.[19, 72] MDA-MB-231 cells were seeded at 5000 cells per well, grown overnight, and incubated for 72 hrs with growth medium containing DOX-4G at final DOX concentrations ranging between 0.005 to 10 μM. As controls, cells were incubated with the equivalent concentrations of free DOX (drug-alone, no nanoparticles), the equivalent protein scaffold concentrations (E2-WT protein nanoparticles alone, no DOX), the same volumes of phosphate buffer alone (no DOX, no nanoparticles), and medium alone. After 72 hr incubation, cells were washed and medium was replaced. MTT in PBS was added to a final concentration of 0.68 mg/mL and incubated at 37°C for 2 hrs. The reaction was terminated

with lysis/solubilization solution (20% w/v sodium dodecyl sulfate in 50:50 dimethylformamide/water, with 2.5% acetic acid and 2.5% 1 N HCl) and incubated at 37 °C overnight. Formazan content was measured by absorbance at 570 nm. Percent cell viability was calculated relative to cells grown in media alone, and a minimum of 3 replicates per concentration was averaged. To calculate the IC_{50}, the data for percent cell viability versus drug concentration was fitted to a four-parameter Hill model. Average IC_{50} values are replicates of three independent experiments.

DOX release from 4-G at pH 5.0

To estimate DOX release from 4-G at pH 5.0, we loaded DOX-4G at pH 7.4 as described above. The buffer was exchanged to pH 7.4 (control) and pH 5.0, the solution was incubated for 48 hr, and free, unbound DOX was removed. The fraction of remaining DOX at pH 5.0 and pH 7.4 was evaluated by fluorescence (using relative fluorescence units) at excitation and emission wavelengths of 478 nm and 594 nm, respectively.

Loading of Nile red and Rhodamine B base in 4-G

We investigated the loading of other two guest molecules, Nile red and rhodamine B base, into the internal cavity of the protein nanoparticle. Purified 4-G and E2-WT (control) were incubated with Nile red or rhodamine B at room temperature for 2 hrs, followed by overnight incubation at 4 °C. Unbound dye molecules were removed by a desalting column. Fluorescence intensities of dye-coupled 4-G and E2-WT were measured for Nile red (excitation 553 nm/emission 636 nm) and for rhodamine B (excitation 540 nm/emission 625 nm).

Supplementary Material

Refer to Web version on PubMed Central for supplementary material.

Acknowledgments

We gratefully acknowledge funding support from NSF (CBET-0827852), NIH (R21 EB010161), and the Department of Defense Breast Cancer Research Program (BC085958) to S.W.W.; an NIH/NLM Pathway to Independence Award (K99LM010821) to A.R.; and NIH (5T15LM007743), NSF (MRI EIA-0321390), and UCI Institute for Genomics and Bioinformatics to P.B. We thank Nicholas Molino for his helpful experimental suggestions. CD, MS, TEM, and confocal microscopy were performed at UCI's Laser Spectroscopy Facility, Mass Spectrometry Facility, Materials Characterization Center, and Optical Biology Core Facility, respectively. Doxorubicin hydrochloride was generously given to us by Dr. Felix Kratz.

REFERENCES

[1]. Langer R, Tirrell DA. Nature. 2004; 428:487. [PubMed: 15057821]

[2]. Zelzer M, Ulijn RV. Chem. Soc. Rev. 2010; 39:3351. [PubMed: 20676412]

[3]. Yan X, Zhu P, Li J. Chem. Soc. Rev. 2010; 39:1877. [PubMed: 20502791]

[4]. Dickerson MB, Sandhage KH, Naik RR. Chem. Rev. 2008; 108:4935. [PubMed: 18973389]

[5]. Nam KT, Kim D-W, Yoo PJ, Chiang C-Y, Meethong N, Hammond PT, Chiang Y-M, Belcher AM. Science. 2006; 312:885. [PubMed: 16601154]

[6]. Vepari C, Kaplan DL. Prog. Polym. Sci. 2007; 32:991. [PubMed: 19543442]

[7]. Flenniken ML, Liepold LO, Crowley BE, Willits DA, Young MJ, Douglas T. Chem. Commun. 2005:447.

[8]. Yan X, Zhu P, Fei J, Li J. Adv. Mater. 2009; 22:1283. [PubMed: 20437520]

[9]. McMillan RA, Paavola CD, Howard J, Chan SL, Zaluzec NJ, Trent JD. Nat. Mater. 2002; 1:247. [PubMed: 12618787]

[10]. Maskarinec SA, Tirrell DA. Curr. Opin. Biotechnol. 2005; 16:422. [PubMed: 16006115]

[11]. Ren D, Kratz F, Wang SW. Small. 2011; 7:1051. [PubMed: 21456086]
[12]. Kratz F. J. Controlled Release. 2008; 132:171.
[13]. McDaniel JR, Callahan DJ, Chilkoti A. Adv. Drug Delivery Rev. 2010; 62:1456.
[14]. Alsenz J, Kansy M. Adv. Drug Delivery Rev. 2007; 59:546.
[15]. Lipinski CA. J. Pharmacol. Toxicol. Methods. 2000; 44:235. [PubMed: 11274893]
[16]. Orlowski S, Garrigos M. Anticancer Res. 1999; 19:3109. [PubMed: 10652600]
[17]. Sikic BI, Fisher GA, Lum BL, Halsey J, Beketic-Oreskovic L, hen G. Cancer Chemother. Pharmacol. 1997; 40(Suppl):S13. [PubMed: 9272128]
[18]. Seelig A. Eur. J. Biochem. 1998; 251:252. [PubMed: 9492291]
[19]. Wang S-W, Monagle J, McNulty C, Putnam D, Chen H. J. Pharm. Sci. 2004; 93:2755. [PubMed: 15389668]
[20]. Yu EW, McDermott G, Zgurskaya HI, Nikaido H, D.E.K. Science. 2003; 300:976. [PubMed: 12738864]
[21]. Rosenberg MF, Callaghan R, Ford RC, Higgens CF. J. Biol. Chem. 1997; 272:10685. [PubMed: 9099718]
[22]. Loo TW, Clarke DM. J. Biol. Chem. 1993; 268:19965. [PubMed: 8104183]
[23]. Izard T, A AE, Allen MD, Westphal AH, Perham RN, de Kok A, Hol WGJ. Proc. Natl. Acad. Sci. U. S. A. 1999; 96:1240. [PubMed: 9990008]
[24]. Dalmau M, Lim S, Chen HC, Ruiz C, Wang SW. Biotechnol. Bioeng. 2008; 101:654. [PubMed: 18814295]
[25]. Dalmau M, Lim SR, Wang SW. Nano Lett. 2009; 9:160. [PubMed: 19113890]
[26]. Dalmau M, Lim S, Wang S-W. Biomacromolecules. 2009; 10:3199. [PubMed: 19874026]
[27]. Molino NM, Bilotkach K, Fraser DA, Ren D, Wang S-W. Biomacromolecules. 2012 In Press.
[28]. Uchida M, Klem MT, Allen M, Suci P, Flenniken M, Gillitzer E, Varpness Z, Liepold LO, Young M, Douglas T. Adv. Mater. 2007; 19:1025.
[29]. Singh P, Gonzalez MJ, Manchester M. Drug Dev. Res. 2006; 67:23.
[30]. Flenniken ML, Uchida M, Liepold LO, Kang S, Young MJ, Douglas T. Viruses and Nanotechnology. 2009; 327:71.
[31]. Duncan R. Nat. Rev. Cancer. 2006; 6:688. [PubMed: 16900224]
[32]. Wong HL, Bendayan R, Rauth AM, Li YQ, Wu XY. Adv. Drug Delivery Rev. 2007; 59:491.
[33]. Launchbury AP, Habboubi N. Cancer. Treat. Rev. 1993; 19:197. [PubMed: 8334677]
[34]. Formariz TR, Sarmento VHV, Silva-Junior AA, Scarpa MV, Santilli CV, Oliveira AG. Colloids Surf., B. 2006; 51:54.
[35]. Dintaman JM, Silverman JA. Pharm. Res. 1999; 16:1550. [PubMed: 10554096]
[36]. Creighton, TE. second ed.. Freeman and Co.; New York: 1993.
[37]. Jackson SE, Moracci M, Elmasry N, Johnson CM, Fersht AR. Biochemistry. 1993; 32:11259. [PubMed: 8218191]
[38]. Chassany O, Urien S, Claudepierre P, Bastian G, Tillement JP. Cancer Chemother. Pharmacol. 1996; 38:571. [PubMed: 8823501]
[39]. Demant EJF, Friche E. Biochem. Pharmacol. 1998; 56:1209. [PubMed: 9802333]
[40]. Castro GR, Larson BK, Panilaitis B, Kaplan DL. Appl. Microbiol. Biotechnol. 2005; 67:767. [PubMed: 15614556]
[41]. Gannon MK, Holt JJ, Bennett SM, Wetzel BR, Loo TW, Bartlett MC, Clarke DM, Sawada GA, Higgins JW, Tombline G, et al. J. Med. Chem. 2009; 52:3328. [PubMed: 19402665]
[42]. Fritze A, Hens F, Kimpfler A, Schubert R, Peschka-Suss R. Biochim. Biophys. Acta, Biomembr. 2006; 1758:1633.
[43]. Savic R, Eisenberg A, Maysinger D. J. Drug Targeting. 2006; 14:343.
[44]. Peer D, Karp JM, Hong S, FaroKHzad OC, Margalit R, Langer R. Nat. Nanotechnol. 2007; 2:751. [PubMed: 18654426]
[45]. Gillies ER, Fréchet JMJ. Bioconjugate Chem. 2005; 16:361.
[46]. Liu SQ, Tong YW, Yang Y-Y. Biomaterials. 2005; 26:5064. [PubMed: 15769542]

[47]. Missirlis D, Kawamura R, Tirelli N, Hubbell JA. Eur. J. Pharm. Sci. 2006; 29:120. [PubMed: 16904301]

[48]. Ren Y, Wong SM, Lim L-Y. Bioconjugate Chem. 2007; 18:836.

[49]. Neidle S, Taylor G. Biochim. Biophys. Acta, Nucleic Acids Protein Synth. 1977; 479:450.

[50]. Izard T, Ævarsson A, Allen MD, Westphal AH, Perham RN, de Kok A, Hol WGJ. Proc. Natl. Acad. Sci. U. S. A. 1999; 96:1240. [PubMed: 9990008]

[51]. Kondo A, Murakami F, Higashitani K. Biotechnol. Bioeng. 1992; 40:889. [PubMed: 18601195]

[52]. Merisko-Liversidge E, Sarpotdar P, Bruno J, Hajj S, Wei L, Peltier N, Rake J, Shaw JM, Pugh S, Polin L, et al. Pharm. Res. 1996; 13:272. [PubMed: 8932448]

[53]. Burgess DJ, Verma S, Kumar S, Gokhale R. Int. J. Pharm. 2011; 406:145. [PubMed: 21185926]

[54]. Pasternack RF, Collings PJ. Science. 1995; 269:935. [PubMed: 7638615]

[55]. Chan G, Mooney DJ. Trends Biotechnol. 2008; 26:382. [PubMed: 18501452]

[56]. Shuai X, Ai H, Nasongkla N, Kim S, Gao J. J. Controlled Release. 2004; 98:415.

[57]. Upadhyay KK, Bhatt AN, Mishra AK, Dwarakanath BS, Jain S, Schatz C, Le Meins J-F, Farooque A, Chandraiah G, Jain AK, et al. Biomaterials. 2010; 31:2882. [PubMed: 20053435]

[58]. Susa M, Iyer A, Ryu K, Hornicek F, Mankin H, Amiji M, Duan Z. BMC Cancer. 2009; 9:399. [PubMed: 19917123]

[59]. Andrew MacKay J, Chen M, McDaniel JR, Liu W, Simnick AJ, Chilkoti A. Nat. Mater. 2009; 8:993. [PubMed: 19898461]

[60]. Gillies ER, Frechet JMJ. Bioconjugate Chem. 2005; 16:361.

[61]. Pichot CS, Hartig SM, Xia L, Arvanitis C, Monisvais D, Lee FY, Frost JA, Corey SJ. Br. J. Cancer. 2009; 101:38. [PubMed: 19513066]

[62]. Jiang W, KimBetty YS, Rutka JT, ChanWarren CW. Nat. Nanotechnol. 2008; 3:145. [PubMed: 18654486]

[63]. Chithrani BD, Ghazani AA, Chan WCW. Nano Lett. 2006; 6:662. [PubMed: 16608261]

[64]. Chithrani BD, Chan WCW. Nano Lett. 2007; 7:1542. [PubMed: 17465586]

[65]. Cedervall T, Lynch I, Lindman S, Berggård T, Thulin E, Nilsson H, Dawson KA, Linse S. Proc. Natl. Acad. Sci. U. S. A. 2007; 104:2050. [PubMed: 17267609]

[66]. Walkey CD, Olsen JB, Guo H, Emili A, Chan WCW. J. Am. Chem. Soc. 2011; 134:2139. [PubMed: 22191645]

[67]. Christie RJ, Grainger DW. Adv. Drug Delivery Rev. 2003; 55:421.

[68]. Mayer LD, Tai LCL, Bally MB, Mitilenes GN, Ginsberg RS, Cullis PR. Biochim. Biophys. Acta. 1990; 1025:143. [PubMed: 2364073]

[69]. Liu Z, Sun X, Nakayama-Ratchford N, Dai H. ACS Nano. 2007; 1:50. [PubMed: 19203129]

[70]. Kabsch W, Sander C. Biopolymers. 1983; 22:2577. [PubMed: 6667333]

[71]. Greenfield NJ. Nat. Protoc. 2006; 1:2527. [PubMed: 17406506]

[72]. Hansen MB, Nielsen SE, Berg K. J. Immunol. Methods. 1989; 119:203. [PubMed: 2470825]

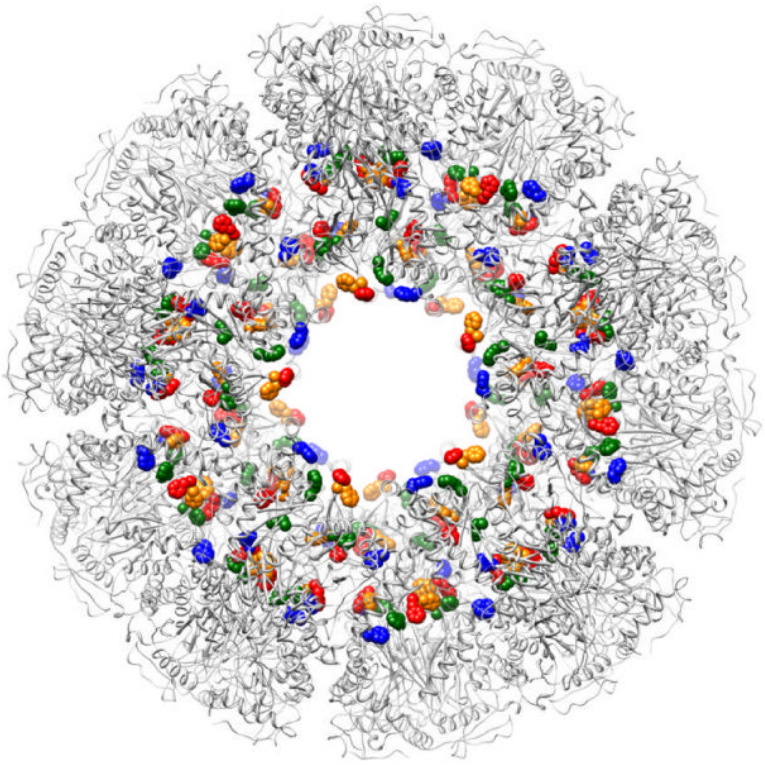

Figure 1.
Fully assembled 60-subunit E2 protein nanoparticle of 4-G quadruple variant (K239F-E375F-R380F-D381F) viewed down the 5-fold axis of symmetry using Chimera. Protein backbone is displayed as ribbons, and Phe side-chains are colored as follows: 239 blue, 375 green, 380 orange, and 381 red.

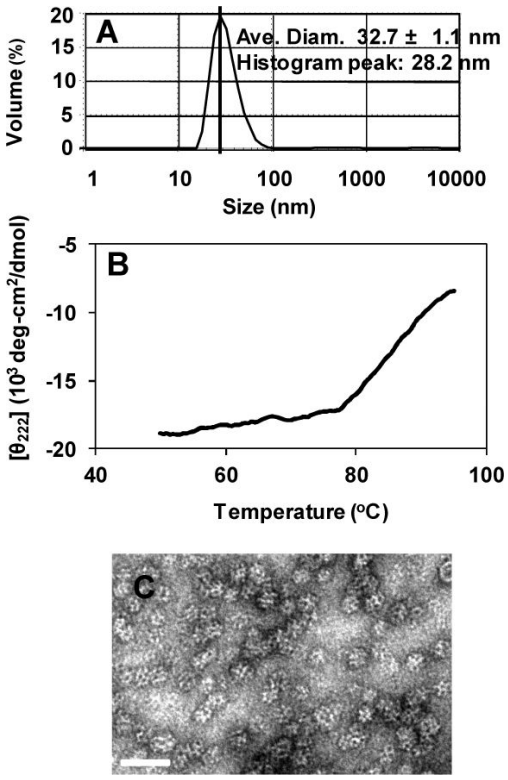

Figure 2.

Representative thermostability and structural characterization of a variant protein scaffold. Presented here is data for K239F-E375F-R380F-D381F (4-G). **A.** Hydrodynamic particle size is ~ 32.7 nm. **B.** Far-UV circular dichroism thermostability scan at 222 nm yields an average T_m of 84.2 °C. **C.** Transmission electron micrograph of samples stained with 2% uranyl acetate. (Scale bar is 50 nm.)

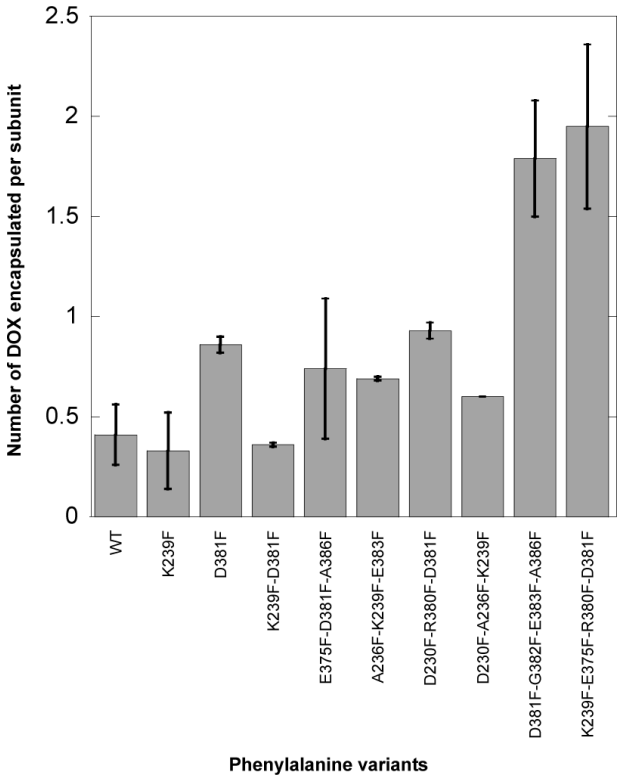

Figure 3.
Number of DOX encapsulated per protein subunit in different Phe variants incubated at a 3:1 DOX:subunit incubation ratio

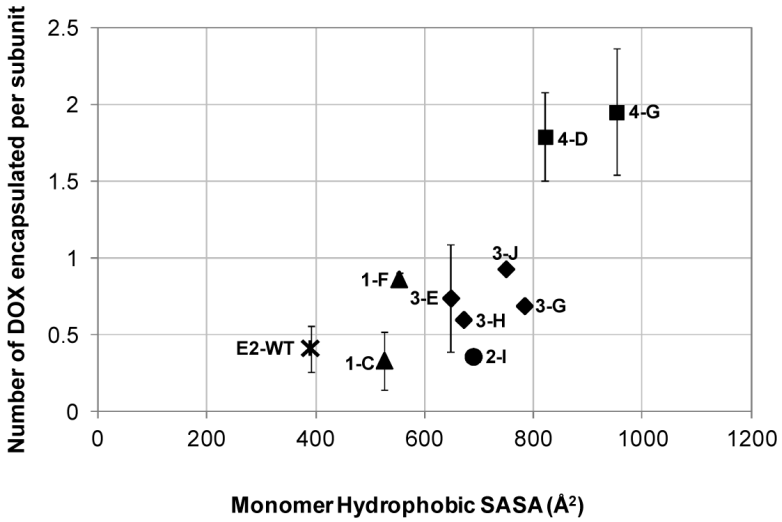

Figure 4.
Number of DOX encapsulated per subunit vs. monomer hydrophobic solvent accessible surface area (SASA) for Phe variants.

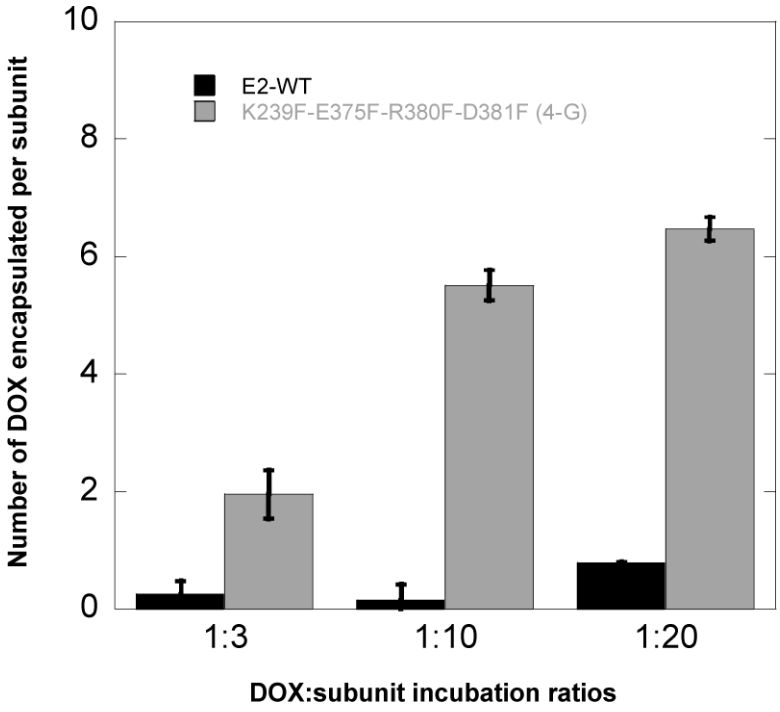

Figure 5.
Number of DOX encapsulated per subunit in E2-WT and K239F-E375F R380F-D381F (4-G) at 3:1, 10:1, and 20:1 DOX:subunit incubation ratios.

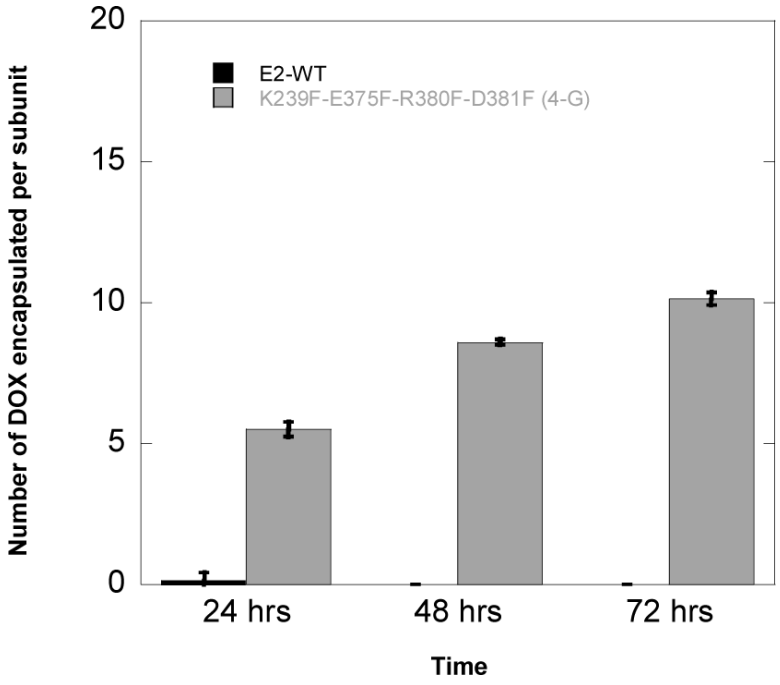

Figure 6.
Number of DOX encapsulated in E2-WT and K239F-E375F-R380F-D381F (4-G) after three successive iterations of 24-hour incubation followed by free-DOX removal. Initial incubation ratio is 10:1 DOX:subunit.

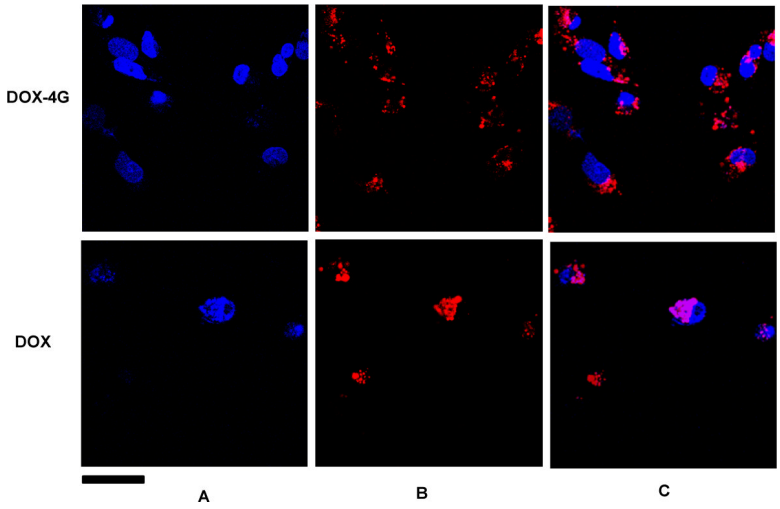

Figure 7.

Confocal laser scanning microscopy images of MDA-MB-231 cells incubated with K239F-E375F-R380F-D381F-DOX (DOX-4G) (top) and free doxorubicin (DOX) (bottom). Nucleus were stained blue with Hoechst 33342 (A), DOX is fluorescent red (B), and overlay of the two (C). Scale bar is 50 μm

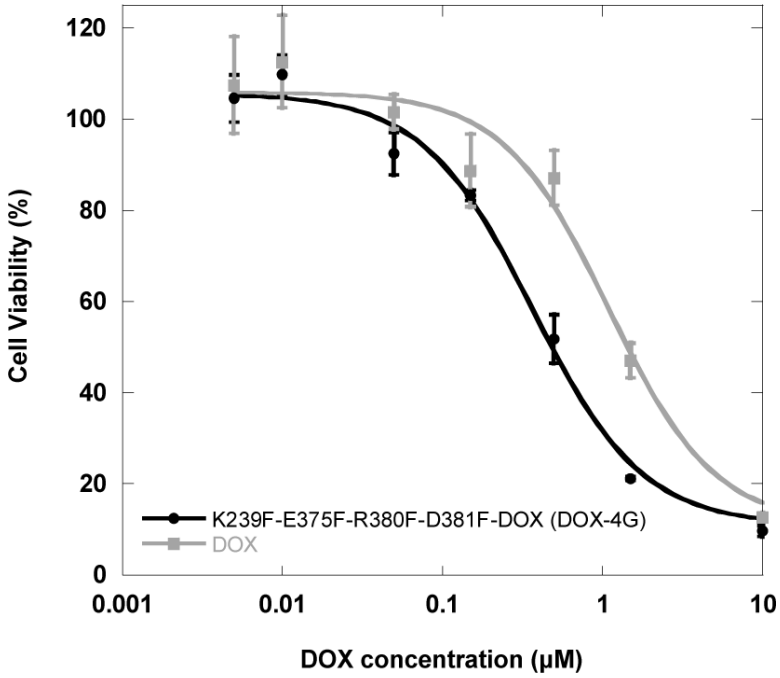

Figure 8.

Dose response curves of MDA-MB-231 incubated with DOX-complexed K239F-E375F-R380F-D381F (DOX-4G) and free doxorubicin (DOX). IC_{50} values are 0.33 ± 0.12 μM and 0.93 ± 0.30 μM for DOX-4G and DOX, respectively.

Table 1

Summary of all Phe variants synthesized

Single-Phe		Double-Phe	
Abbreviation	**Mutations***	**Abbreviation**	**Mutations**
1-A	D230F	2-A	R380F-D381F
1-B	A236F	2-B	D381F-G382F
1-C	K239F	2-C	D381F-E383F
1-D	E375F	2-D	E375F-D381F
1-E	R380F	2-E	E375F-A386F
1-F	D381F	2-F	G382F-A386F
1-G	G382F	2-G	A236F-K239F
1-H	E383F	2-H	D230F-R380F
1-I	A386F	2-1	K239F-D381F

Triple-Phe		Quadruple-Phe	
Abbreviation	**Mutations**	**Abbreviation**	**Mutations**
3-A	R380F-D381F-G382F	4-A	R380F-D381F-G382F-E383F
3-B	D381F-G382F-E383F	4-B	R380F-G382F-E383F-A386F
3-C	R380F-D381F-E383F	4-C	E375F-R380F-D381F-G382F
3-D	E375F-R380F-D381F	4-D	D381F-G382F-E383F-A386F
3-E	E375F-D381F-A386F	4-E	K239F-R380F-D381F-G382F
3-F	G382F-E383F-A386F	4-F	E375F-D381F-G382F-A386F
3-G	A236F-K239F-E383F	4-G	K239F-E375F-R380F-D381F
3-H	D230F-R380F-D381F	4-H	A236F-K239F-G382F-E383F
3-I	E375F-E383F-A386F	4-I	D230F-A236F-K239F-D381F
3-J	D230F-A236F-K239F		

* For all mutations, the first letter is the standard single-letter amino acid abbreviation for the original sequence,[36] the number following it is the site location, and F is the Phe to which the amino acid has been mutated.

Table 2

Size and stability of purified E2 Phe variants

Variant Abbreviation	E2 Scaffold Mutation	Diameter (nm)	T_m (°C)	T_o (°C)
E2-WT	Wild Type (control, no mutation)	26.9 ± 0.7	90.1 ± 1.5	79.2 ± 1.6
1-C	K239F*	30.4 ± 0.9	89.1 ± 0.8	77.1 ± 0.8
1-F	D381F*	25.9 ± 1.0	90.6 ± 1.0	79.8 ± 0.2
2-1	K239F-D381F*	26.2 ± 0.4	89.0 ± 0.9	77.7 ± 0.9
3-E	E375F-D381F-A386F	27.4 ± 0.6	83.3 ± 0.6	74.6 ± 0.2
3-G	A236F-K239F-E383F	26.0 ± 0.7	89.0 ± 0.2	78.8± 1.3
3-H	D230F-R380F-D381F	27.5 ± 0.4	85.7 ± 0.5	76.3 ± 1.0
3-J	D230F-A236F-K239F	27.2 ± 3.7	83.8 ± 0.3	77.5 ± 0.5
4-D	D381F-G382F-E383F-A386F	27.4 ± 4.5	83.9 ± 0.4	66.7 ± 2.5
4-G	K239F-E375F-R380F-D381F	32.7 ± 1.1	84.2 ± 0.7	73.5 ± 1.6

T_m: Midpoint temperature of unfolding; T_o: Onset temperature of unfolding.

*Data with asterisk are from Dalmau *et al.,* 2008.[24]